

Open Access: ISSN 1847-9286 www.jESE-online.org

Original scientific paper

Iron-rich industrial sludge-derived metal organic framework for enhanced photoelectrochemical degradation of methylene blue

Nurul Athikah Azizan¹, Norhaslinda Nasuha¹,⊠, Hawaiah Imam Maarof¹, Suriati Sufian² and Wan Izhan Nawawi Wan Ismail³

¹School of Chemical Engineering, College of Engineering, Universiti Teknologi MARA, 40450 Selangor, Malaysia

²Chemical Engineering Department, Universiti Teknologi PETRONAS, Bandar Sri Iskandar, 32610 Sri Iskandar, Perak, Malaysia

³Faculty of Applied Sciences, Universiti Teknologi MARA, 02600 Arau, Perlis, Malaysia Corresponding author: [™]norhaslinda.nasuha@uitm.edu.my; Tel.: +6010-4043426

Received: August 8, 2025; Revised: October 16, 2025; Published: October 18, 2025

Abstract

The escalating discharge of textile effluents, burdened with persistent dyes such as methylene blue (MB), has become a significant global concern. In this study, a surface-engineered iron sludge, denoted as IMS-MOF, was synthesized by modifying iron-rich industrial metal sludge (IMS) to enhance its performance in photoelectrochemical degradation of MB. The IMS-MOF was synthesized via a hydrothermal method, utilizing IMS as the metal ion source and 1,3,5-tricarboxylic acid (BTC) as ligand. Characterization results revealed that IMS-MOF exhibited an increase in surface area (50.34 m² g⁻¹), and porosity (0.27 cm³ g⁻¹) compared to IMS (36.56 m^2 q^{-1} , 0.19 cm³ q^{-1}). Additionally, the MOF process induced a morphological transition from densely agglomerated particles with rough surface features to well-defined, rod-shaped crystalline structures, characteristic of metal-organic frameworks, thereby significantly enhancing the specific surface area and active site accessibility. This structural rearrangement led to a significant increase in the specific surface area and facilitated enhanced access to the active sites within the framework. The band gap reduction in IMS-MOF enhanced its photocatalytic activity under UV light irradiation. Photoelectrochemical degradation studies showed that IMS-MOF achieved higher MB removal efficiency than IMS, with over 90 % MB degradation within a specific contact time. The adsorbent exhibits good adsorption performance over a broad pH range (5-11). By scavenging tests of free radicals generated, hydroxy radicals (·OH) and superoxide radicals (·O²-) were indicated as the reactive oxygen species in the photoelectrochemical degradation. Although IMS-MOF showed a 15.1 % decrease after 10 cycles, it still possessed reusability and stability, indicating that it is qualified for textile wastewater treatment in practice.

Keywords

Heterogeneous catalyst; industrial waste-derived materials; surface modification; advanced oxidation process; dye-contaminated wastewater

Introduction

Textile dyeing effluents containing rich chromophoric compounds have a significant impact on the attenuation of photosynthetically active radiation (PAR) in aquatic ecosystems [1]. This reduction of PAR could interrupt the phototrophic metabolism of primary producers, leading to a trophic interruption in aquatic food webs and an increased risk of anthropogenic diseases [2,3]. Textile dyeing effluents have been reported to contain high concentrations of organic pollutants that are almost recalcitrant in nature and likely toxic [4,5]. The textile wastewater should be processed in accordance with environmental laws and regulations before being discharged to avoid pollution and minimize environmental risks.

Textile dyeing wastewater is treated by a combination of technologies, such as physical [6,7], chemical [8,9], and biological processes [10], to achieve discharge quality standards [11]. Photoelectrochemical advanced oxidation processes (PEC-AOPs) degradation is one of the new approaches for the degradation of dye synthetic compounds in wastewater treatment, in which the coupling of photocatalyst and electrochemical reactions takes place [11]. This simultaneous reaction utilizes light energy to initiate the oxidative degradation of organic pollutants, which exist in high concentrations in effluent wastes generated from the textile industry, that are a huge environmental concern because of the environmental toxicities of synthetic dyes [12]. The PEC-AOPs systems for the treatment of wastewater have numerous advantages. Better charge carrier separation with an imposed external bias leads to more powerful formation of reactive oxygen species (ROS) that are able to degrade the existing contaminants [13]. In recent years, there has been great progress towards the development of more advanced PEC-AOPs via bias-free ionassisted methods, which can realize a considerable enhancement of the energy efficiency [14]. PEC-AOPs are also capable of complete mineralization of organic contaminants to non-toxic substances with minimal-to-no generation of toxic or hazardous intermediates [15]. As PEC-AOPs systems are resistant to a wide range of environmental parameters (e.g. pH, ionic strength), they can be more widely adopted in real-world wastewater treatment [16].

This paper presents a new recycling industrial waste product, the iron-rich industrial metal sludge (IMS), which is applied in environmental remediation and in the synthesis of composite and catalytic materials. However, its implementation is impeded by several key factors. Metal ion leaching can lead to environmental pollution and affect the stability of materials, so this is also one of the main problems [17]. Furthermore, the untreated IMS with relatively small specific surface area, insufficient active sites and poor structural stability is also restricted in use for adsorption or catalytic reactions [18]. To address these shortcomings, surface and structural modifications are necessary to enhance the functional properties of IMS and inhibit metal release. The application as a PEC catalyst for dye wastewater and industrial waste treatment of dye using IMS is also a possible application. Although it exhibits higher catalytic reactivity and improved kinetic performance compared to IMS, the latter still shows limited activity and a slower degradation rate than more advanced catalytic materials. Although composites such as cellulose/Fe-MOF [19], MOF-IO [20], Fe-MOF@MoS₂ [21] and Fe₃O₄@SiO₂ [22] have shown improved performance, IMS materials still experience degradation through corrosion and oxidation, which limits their recyclability. Therefore, to enable the effective application of IMS in environmental systems, comprehensive strategies to strengthen its structure and stability are essential. IMS waste is difficult to manage and dye selectivity in IMS might be insufficient for the complete treatment of complex waste streams [23,24]. However, advancements in material engineering and hybrid systems may enhance IMS in PEC.

Metal-organic frameworks (MOFs) are known as one of the most promising materials for tuning structural and functional properties because of their large surface area, scalable porosity, and chemical modifiability [25-27]. To address the intrinsic drawbacks of IMS, such as instability and Fe leaching during catalytic processes, an alternative MOF approach using trimesic acid (1,3,5-benzene-tricarboxylic acid, BTC) has been adopted to assemble an IMS-MOF heterostructure. This approach not only contributes to the mechanical stability and catalytic performance of IMS, particularly in photoelectrochemical (PEC) dye degradation, but also solves a serious problem of metal ions leaching that impedes the practical application of the unmodified IMS [28,29]. In IMS-MOF, iron ions serve as central metal nodes in the crystal system of MOFs, thereby possessing not only the catalytic activity of iron but also being highly porous and tuneable MOFs [30]. Such a synergetic combination brings vast application potentials in environmental treatment and heterogeneous catalysis.

The fundamental significance of this work is to propose an environmentally benign strategy for reusing IMS waste as precious catalytic materials. This not only offers a cost-effective and sustainable strategy for the treatment of industrial sludge but also supplies an alternative route for durable MOF-derived catalysts in wastewater purification. By combining waste-to-resource utilization with high catalytic activity, this work proposes advancements in the circular economy and the development of MOF-based environmental treatment technologies.

In this study, a novel catalyst named IMS-MOF is prepared using a hydrothermal MOF method, with IMS as the driving agent. The cooperating of IMS nodes and BTC linkers forms a stable IMS-MOF, which functional groups and intermolecular interaction are characterized by scanning electron microscopy (SEM), x-ray photoelectron spectroscopy (XPS), Fourier transform infrared spectroscopy (FTIR), isoelectric point (IEP), cyclic voltammetry (CV), electrochemical impedance spectroscopy (EIS), linear sweep voltammetry (LSV) techniques. The recyclability of the IMS-MOF catalyst is also examined for the long term. The main purpose of the present work is to assess the capability of IMS-MOF as a green, efficient and clean catalyst in the PEC process for MB dye degradation, which provides both research novelty and engineering applications.

Experimental

Materials

Iron-metal-sludge (IMS) was procured from a steel factory in Shah Alam, Selangor, Malaysia, and served as the precursor for synthesizing an IMS-MOF. All other chemicals employed in this investigation were of analytical grade and acquired from Sigma-Aldrich. Ultrapure deionized water with a resistivity of $18.2~\mathrm{M}\Omega\mathrm{\cdot cm}$ was utilized for the preparation of all aqueous solutions. Benzene-1,3,5-tricarboxylic acid (Trimesic acid, BTC) and N, N-dimethylformamide (DMF) were utilized as the organic linker and solvent, respectively, in the IMS-MOF preparation. The supporting electrolyte was made up of a sodium chloride (NaCl) solution. $0.1~\mathrm{M}$ aqueous solutions of sodium hydroxide (NaOH) and hydrochloric acid (HCl) were employed to alter the pH of the solutions to the desired value. A stock solution of methylene blue (MB) was prepared (200 ppm).

Preparation of IMS-MOF

The IMS was first sieved to discard debris and other contaminants. It was then washed successively, followed by filtration to remove impurities and fine particulates. The washed IMS was dried in an oven at 80 °C overnight and finally calcined at 450 °C in a furnace for 2 hours, to transform all iron-containing species present in the IMS into iron oxide. The preparation of IMS-MOF was modified from [28]. A hydrothermal method was used, whereby 1.246 g of IMS and 1.937 g of BTC were mixed with a certain

volume of DMF with a precursor-to-solvent molar ratio, IMS: BTC: DMF = 1:2:400. The resulting mixture was then transferred to a 250 mL Teflon-lined stainless-steel autoclave and subjected to hydrothermal treatment at 150 °C for 24 h. The resulting product was a blackish powder, obtained after thorough washing, filtration, and subsequently drying at 80 °C for 2 hours, as illustrated in Figure 1. This process yielded the desired IMS-MOF material.

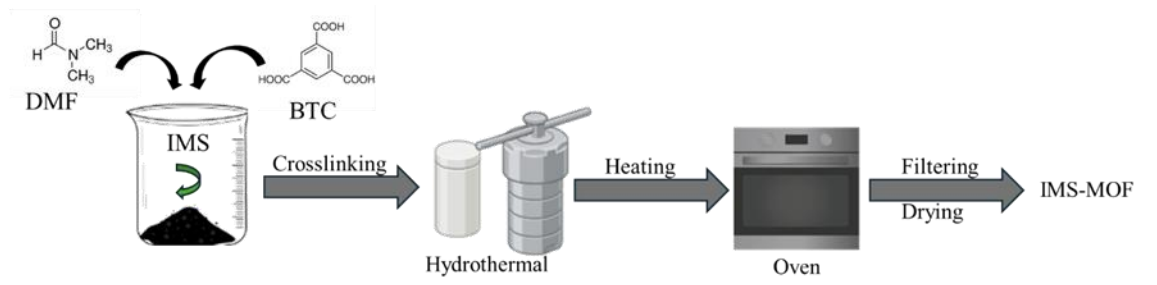


Figure 1. Schematic illustration of the IMS-MOF preparation

IMS-MOF performance of oxidizing organic compounds

This study investigates the electrocatalytic degradation of MB dye in aqueous solution using the IMS-MOF catalyst. Experiments were conducted in a 100 mL electrochemical cell equipped with a platinized titanium anode and a carbon cathode. A 50 ppm MB solution was employed, with the addition of 1 M NaCl to enhance conductivity. The cell was maintained at a constant stirring speed of 160 rpm for 180 minutes. A direct current (DC) power supply was used to apply a constant current density of 1 mA cm⁻². Before the photoelectrochemical process, the system has equilibrated in the dark for 20 minutes for the adsorption-desorption equilibrium between MB dyes and IMS-MOF catalyst. Different factors like catalyst dosage (0.01 to 0.06 g L⁻¹), initial pH (2-7) and initial MB concentration (25 to 150 ppm) were studied to observe their impact on the degradation performance. Catalyst recyclability and metal leaching were further investigated. UV-Vis spectroscopy was used to monitor the progress of the reaction, and each experiment was performed in triplicate. Removal, % of MB was calculated using Equation (1):

$$Removal = \frac{C_i - C_f}{C_i} 100 \tag{1}$$

where C_i and C_f / mg L⁻¹ are the initial and final concentrations of the MB dye in the liquid phase.

Characterization of IMS-MOF

Following the preparation of the IMS-MOF, the materials were comprehensively characterized using a suite of analytical techniques. These included scanning electron microscopy with energy-dispersive X-ray spectroscopy (SEM-EDX, DSM 982 GEMINI) for morphological and elemental analysis, Fourier-transform infrared spectroscopy (FTIR, Perkin Elmer) for functional group identification, Brunauer-Emmett-Teller (BET, 3FLEX 3500) analysis for surface area and porosity determination, X-ray diffraction (XRD, Rigaku Model Ultima IV) for crystallographic structure elucidation, X-ray photoelectron spectroscopy (XPS, Axis Ultra DLD) for surface chemical composition and to investigate surface reactivity and oxygen desorption behaviour, and ultraviolet-visible diffuse reflectance spectroscopy (UV-Vis DRS, Cary 5000) for optical property and band gap analysis.

Determination of isoelectric point

The isoelectric point (IEP) of the IMS-MOF material was determined using a Malvern Zetasizer Nano-series. To establish a pH gradient, 100 mL solutions of 0.25 M NaCl, 0.25 M HCl and 0.025 M HCl were prepared, and their initial pH values were adjusted within the range of 2 to 7. Following

treatment, aliquots of the solutions were transferred to zeta potential measurement cells. The final pH of each solution was recorded, and a plot of zeta potential *versus* pH was constructed. The IEP of the IMS-MOF material was determined as the point of zero charge (PZC), identified as the pH value at which the zeta potential intersects the x-axis.

Electrochemical studies

A screen-printed carbon electrode (SPCE) was used to carry out electrochemical experiments. The supporting electrolyte, comprising 0.1 M KCl and 5 mM potassium ferrocyanide (K₄[Fe(CN)₆]), served as a redox probe to evaluate the electron transfer characteristics of the electrode surface. A portion of this electrolyte solution was mixed with IMS-MOF and cast onto the working electrode of SPCE. Electrochemical measurements were subsequently carried out on a Metrohm Autolab potentiostat and interfaced with NOVA 1.10 software for data acquisition and analysis. The same experimental strategy was applied for the collection of electrochemical impedance spectroscopy (EIS), cyclic voltammetry (CV), and linear sweep voltammetry (LSV) studies.

Scavenger experiment

The major reactive oxygen species (ROS) engaged in MB degradation were confirmed. Under UV irradiation, the reaction mixture contained MB and the IMS-MOF catalyst. To ascertain the main ROS, 1 mM of various scavengers was added to the reaction system. Ethylenediaminetetraacetic acid disodium salt (EDTA-2Na) was used to trap positively charged holes (h^+), and hydrogen peroxide (H_2O_2) preferentially quenched hydroxyl radicals (·OH) in this study. Superoxide anion radicals (·O $_2$ -) were trapped by using p-benzoquinone (PBQ), and silver nitrate (AgNO $_3$) was used as an electron scavenger.

Results and discussion

Characterization of the catalyst

The X-ray diffraction (XRD) analysis of IMS-MOF (Figure 2a) revealed a highly crystalline material with a predominant magnetite (Fe₃O₄) phase, with characteristic diffraction peaks at 32.0, 35.6, 41.5, 57.3 and 62.7° matching the standard magnetite reference (ICD: PDF 01-084-2782). The XRD pattern exhibited similarities to analogous frameworks such as Fe complexes [29], i-MOF [30], BC@MIL--88B(Fe) [31], and HKUST-1 [32], suggesting a common structural motif. Additionally, these results confirm the successful incorporation of Fe₃O₄ nanoparticles within the MOF matrix. Comparative analysis with the unmodified IMS precursor revealed a partial transformation of the hematite (Fe₂O₃) phase to magnetite, likely due to the interaction between BTC (organic linker) and the iron species. This interplay alters the oxidation state of iron, promoting the reduction of iron and causing the observed phase transition, which exemplifies the strong effect of the synthesis process on the structural and compositional properties of the material [33,34]. FTIR spectra shown in Figure 2b were employed to analyse the functional groups of IMS and IMS-MOF. The band of 1600 cm⁻¹ can be attributed to the stretching vibrational C=C, indicating the existence of aromatic rings in IMS--MOF [29]. The band appearing at 1400 cm⁻¹ corresponds to the symmetric stretching of the carboxyl(-COOH) functional group [35], which also indicates the successful incorporation of BTC into IMS-MOF. Furthermore, the absorption band at about 1000 cm⁻¹ was found to be related to the C-H deformation vibrations, which are of a higher intensity in the profile of IMS-MOF, indicating a particular change in an organic framework [36]. The detected peaks situated at lower wavenumber at ≈500 cm⁻¹ can be ascribed to the Fe-O stretching vibrational modes, thus establishing the presence of Fe-organic complexes within IMS-MOF [35]. The changed positions of the Fe-O band relative to that of IMS indicate structural modifications associated with the binding of the BTC linker to the Fe species. The absence of the free carboxylic C=O stretch at ≈1700 cm⁻¹ demonstrates that BTC is deprotonated and coordinated to Fe sites [37]. This coordination formation further supports that the organic linker is effectively incorporated with the iron species in the IMS-MOF framework, resulting in stronger Fe-O-C bonding. The above bonding type indicates that a strong coupled effect between BTC and Fe was formed in the composite, and the ligand not only acted as a stabilizer for the metal node but also facilitated electron delocalization. This stronger interaction facilitates better light absorption and charge transfer, which is responsible for the superior photocatalytic efficiency of the IMS-MOF.

These significant changes in band intensities, along with the alterations in C=C, C-H, and Fe-O bonding compared to pure IMS, further confirm the successful synthesis of IMS-MOF and the effective incorporation of organic ligands into the Fe-based material.

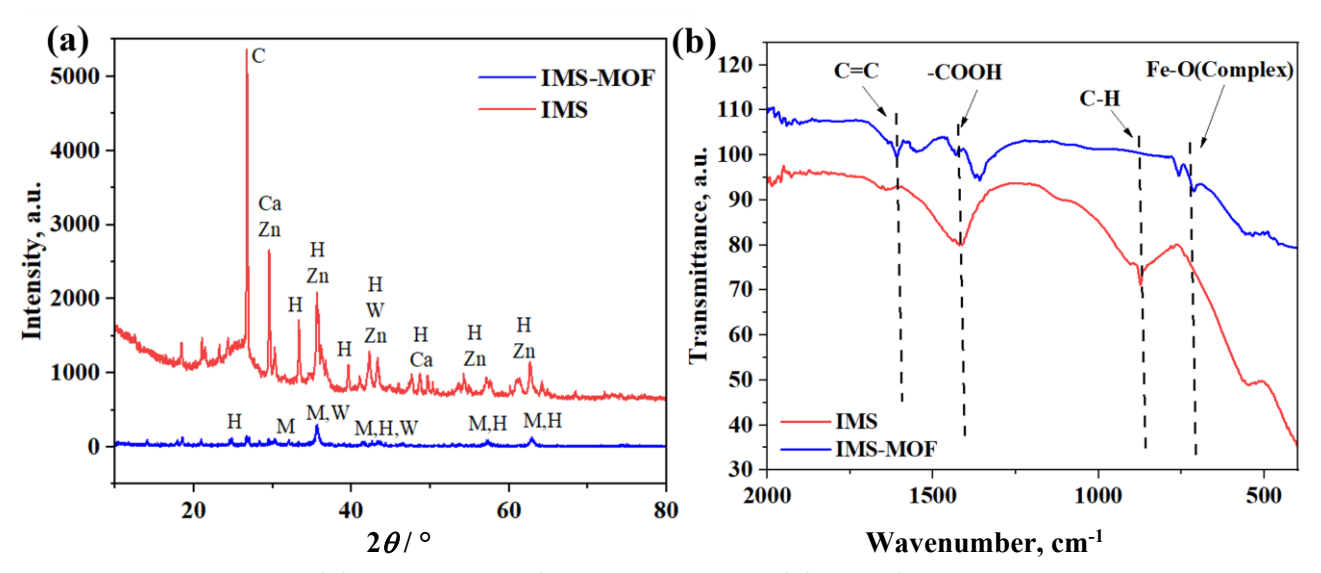


Figure 2. (a) XRD patterns of IMS and IMS-MOF, (b) FTIR of IMS and IMS-MOF

The surface morphology of IMS and IMS-MOF, as observed in Figure 3(a,b), reveals significant changes after modification with the BTC linker. IMS (Figure 3a) exhibits agglomerated, densely packed particles with a rough surface texture, indicative of a limited surface area and a paucity of accessible active sites. This compact morphology likely impedes the adsorption of organic pollutants, consequently affecting degradation efficiency. Conversely, IMS-MOF (Figure 3b) displays well-defined, rod-like crystalline structures characteristic of metal-organic frameworks. This morphological transformation suggests an increase in surface area, affording a greater number of active sites and enhancing the material's adsorption capacity.

Both IMS and IMS-MOF exhibit Type IV isotherms with a distinct hysteresis loop, classifying them as mesoporous materials according to the IUPAC classification. The presence of a hysteresis loop during the intermediate stages of adsorption and desorption, coupled with a saturation plateau at high relative pressure, further substantiates the mesoporous character of both materials. Because the textural properties of both IMS and IMS-MOF were analysed by nitrogen adsorption-desorption isotherms, there were significant differences between the two materials. The BET specific surface area of IMS was 36.56 m² g⁻¹, pore volume was 0.19 cm³ g⁻¹, and average pore size was 13.03 nm.

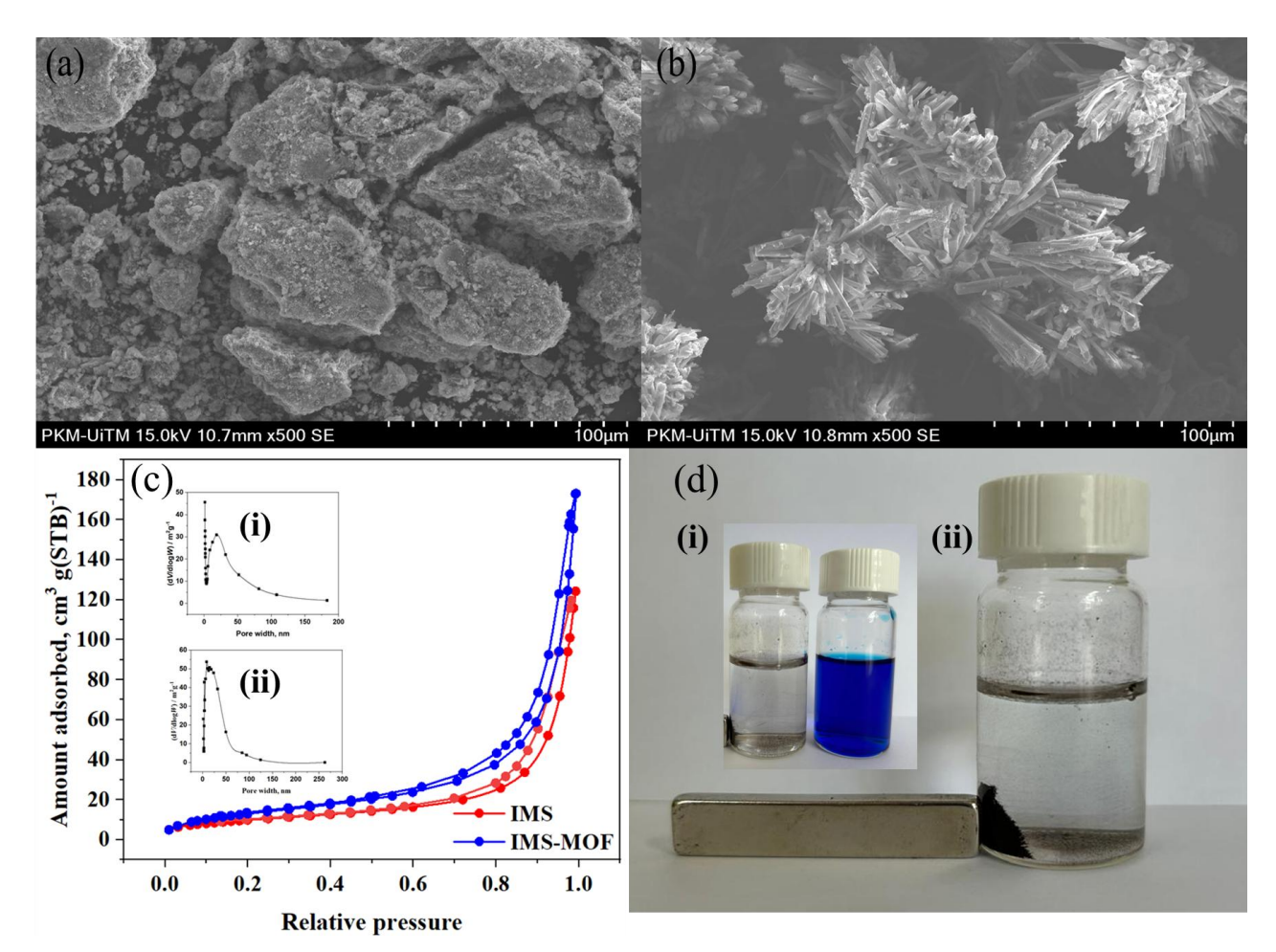


Figure 3. SEM images of (a) IMS and (b) IMS-MOF; (c) N_2 adsorption—desorption isotherms and corresponding pore size distributions of (i) IMS and (ii) IMS-MOF, where V denotes the volume of N_2 adsorbed (cm³ g⁻¹ STP⁻¹) and W represents the pore width (nm); (d) magnetic recovery of IMS-MOF, where (i) shows the solution before and after methylene blue (MB) degradation, and (ii) demonstrates the facile magnetic separation of the IMS-MOF catalyst from the reaction medium using an external magnet

The BET specific surface area of the new material IMS-MOF significantly increased from 6.04 to $50.34~\text{m}^2~\text{g}^{-1}$ after stepwise modification with the BTC linker, and the pore volume increased to $0.27~\text{cm}^3~\text{g}^{-1}$ with the average pore size of 15.5 nm. However, the textural properties of the IMS-MOF material represent an enhancement from those of the parent IMS, yet the obtained surface area of $50.34~\text{m}^2~\text{g}^{-1}$ is significantly lower than those reported for conventional Fe-BTC MOFs (800 to $1400~\text{m}^2~\text{g}^{-1}$) [38]. Several factors explain this difference. In the first place, the embedding of IMS within the MOF matrix might induce structural defects or compromise the long-range order of the crystalline structure, restricting the total porosity [39]. Secondly, potential pore blockage by residual metal sludge components from the IMS precursor could contribute to the diminished surface area, as these particles may occupy or obstruct the accessible pore network.

The interaction between Fe sites in IMS and IMS-MOF with the BTC linker significantly influences the electronic structure, which in turn affects their catalytic properties. This interaction was further explored using XPS analysis. The survey spectra (Figure 4 (a, b)) confirm the presence of Fe, O, and C in both IMS and IMS-MOF. The Fe 2p high-resolution spectra provides insights into the oxidation state and electronic structure of Fe in both materials. In IMS (Figure 4a), Fe $2p_{3/2}$ and Fe $2p_{1/2}$ peaks are observed at 705.4 and 718.5 eV, respectively, indicating the presence of Fe³⁺ species. The broad peak shape suggests the coexistence of multiple oxidation states, likely due to surface hydroxylation or adsorbed oxygen species. The observed separation of ~13 eV between Fe $2p_{3/2}$ and Fe $2p_{1/2}$ is consistent with Fe-based

compounds, further confirming the presence of Fe species in the material. After MOF functionalization (Figure 4b), a blue shift is observed in Fe 2p binding energies, with Fe $2p_{3/2}$ and Fe $2p_{1/2}$ shifting to 708.9 and 721.9 eV, respectively. This shift suggests a ligand-induced charge transfer effect, where the coordination of Fe with the BTC linker alters its electronic environment. Such charge transfer reduces the recombination rate of charge carriers and promotes charge separation, which is beneficial for catalytic applications. Similar trends have been reported in Fe-based catalysts, where the coordination of organic ligands modulates Fe-oxidation state and enhances electron mobility.

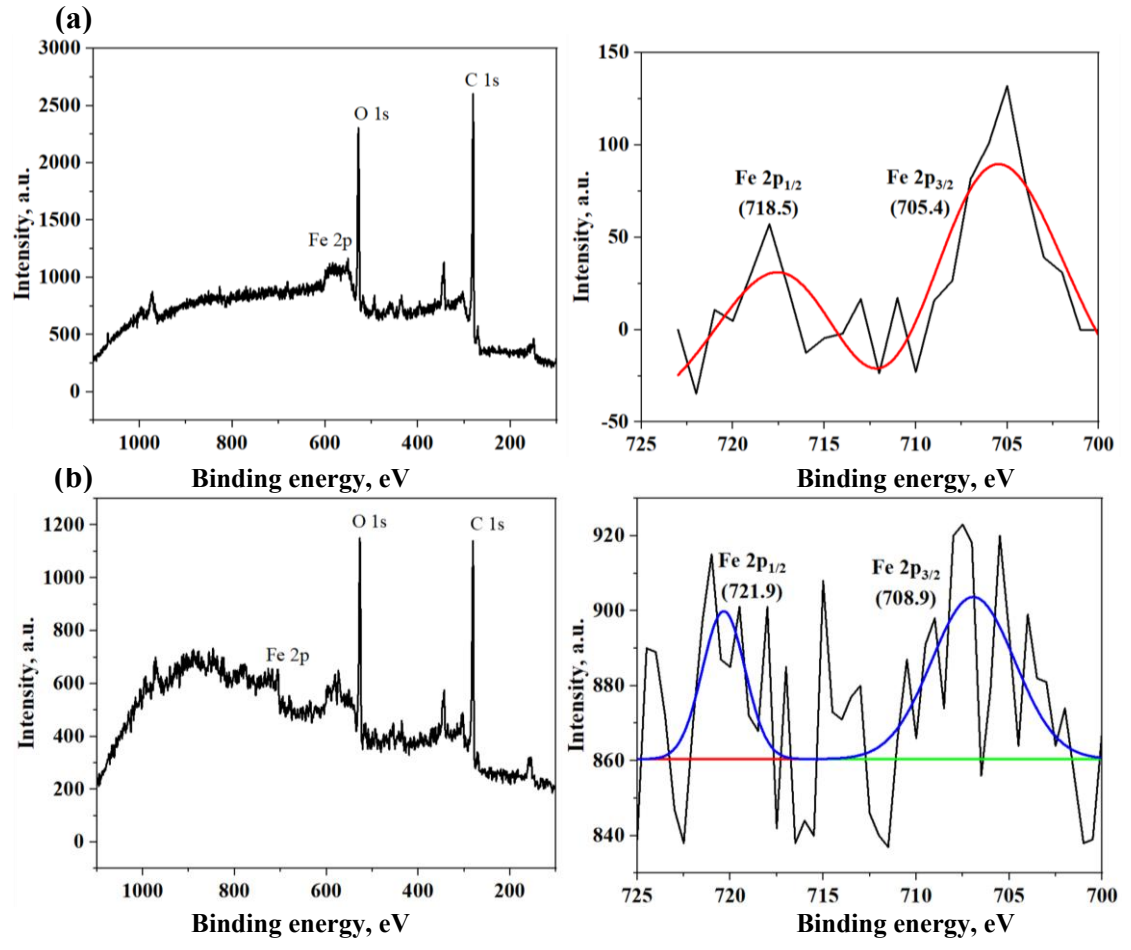


Figure 3. XPS spectra of (a) IMS and (b) IMS-MOF

Furthermore, the deconvolution of Fe 2p spectra in IMS-MOF suggests increased covalency in Fe-O bonding can influence adsorption properties and catalytic performance. The shift in Fe binding energies, along with the modified electronic structure, supports the hypothesis that BTC ligands play a crucial role in stabilizing Fe active sites and tuning their redox properties. These electronic modifications in IMS-MOF highlight the role of BTC functionalization in enhancing charge separation, increasing active sites, and potentially improving photocatalytic efficiency.

The magnetic recovery of the IMS-MOF was confirmed by its facile magnetic separation using an external magnet, as demonstrated in Figure 3d(ii). This attribute enables efficient catalyst recovery and reuse, which is a critical advantage for practical applications in wastewater treatment and environmental remediation. It promotes sustainable catalyst utilization and minimizes potential secondary pollution.

Isoelectric point studies

The presence of BTC as an organic linker significantly influences the surface charge characteristics of MOF. Before modification with BTC, the IMS material exhibited isoelectric points (IEP) at pH 11.8

and pH 12 as shown in Figure 5, with corresponding zeta potentials of 0.1 and 0.3 mV, respectively. This shows that the material's surface was nearly neutral in this pH range with very low electrostatic repulsion in solution. After being modified with BTC (IMS-MOF), the IEP moved to pH 5.32. The significant change is due to the addition of BTC, which carries pH-sensitive carboxyl groups (-COOH) [30]. These groups undergo deprotonation at elevated pH, forming negatively charged carboxylate groups (-COOT) and thus endowing the modified material with more negative charge [30,40]. A zeta potential of 6 mV was recorded after modification, which also promotes this behaviour due to increased electrostatic interactions with the surrounding medium. These significant changes in the surface charge properties are expected to affect the material's performance in MB dye degradation, as electrostatic interaction is a major factor governing adsorption and the degradation process [28].

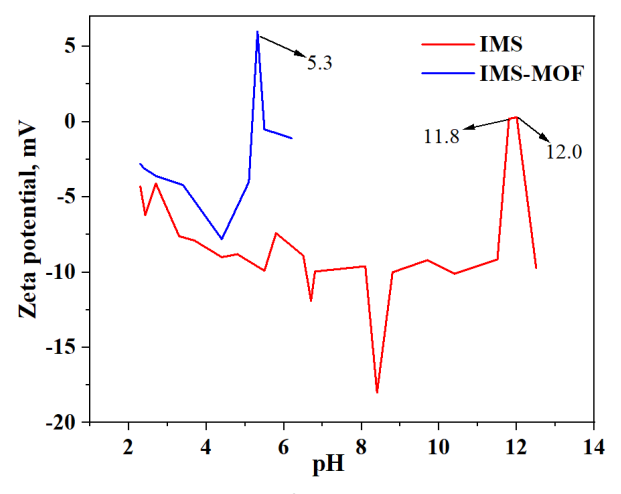


Figure 4. IEP of IMS and IMS-MOF

Band gap studies

As shown in Figure 6, the resulting Tauc plot indicated a substantially lowered band gap of 2.09 eV for IMS-MOF, in contrast to the band gap of 3.05 eV for IMS material. The decrease in band gap is due to the presence of the BTC linker in the MOF structure [41]. The linker BTC, as an electron-rich organic ligand, contributes to improved electronic delocalization [42]. Specifically, the BTC linker contains an aromatic skeletal structure, which introduces new electronic energy levels, joint between the valence and conduction bands, greatly reducing the amount of energy required to excite electrons [43]. The introduction of the BTC linker into the IMS framework fundamentally alters its electronic structure through the formation of Fe-O-C coordination bonds. These bonds extend the conjugation between the Fe centres and the aromatic carboxylate ligand, enabling electron delocalization across the inorganic-organic interface. As a result, mid-gap states are generated within the band structure, effectively narrowing the optical band gap and shifting the absorption edge toward the visible-light region. This band gap modulation enhances the ability of IMS-MOF to harvest visible photons and facilitates more efficient electron excitation. The synergistic interaction between Fe active sites and the π -conjugated BTC ligand, therefore, transforms IMS from a UV-responsive material into a photoactive system capable of driving visible-light-induced photocatalysis with improved charge separation and reduced recombination losses.

The IMS absorber exhibited low visible spectrum absorbance. The wide band gap and lack of π -conjugated structure required for highly efficient light harvesting in this range result in this low visible light absorption [44]. In contrast, the visible absorbance of the IMS-MOF catalyst was much stronger and broader. The introduction of the BTC linker directly modifies the electron band, thus endowing it with enhanced visible light absorption capability [45]. The BTC linker endows the IMS-

MOF with a charge transfer process, contributing to its light-harvesting capability. Apart from enhancing sunlight capture in the visible region, the BTC linker plays a role in stabilizing the electronic structure of the material [46]. This stability results in low recombination speeds of photogenerated electron-hole pairs, which is an important factor in improving photocatalytic efficiency.

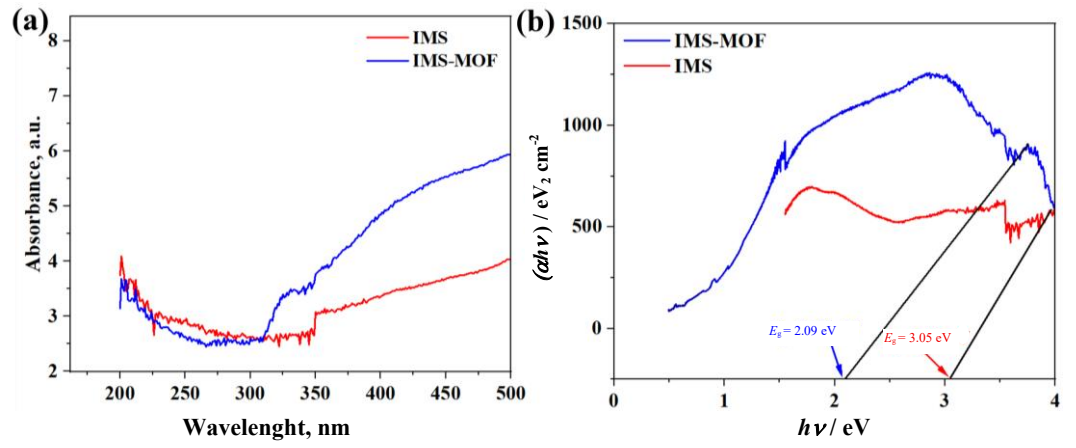


Figure 5. UV-Vis diffuse reflectance spectra (UV-Vis DRS) and corresponding Tauc plots of IMS and IMS-MOF: (a) comparative UV-Vis DRS spectra of IMS and IMS-MOF, (b) Tauc plots of IMS and IMS-MOF showing reduction in band gap energy

Electrochemical characterization

Cyclic voltammetry (CV), electrochemical impedance spectroscopy (EIS), and linear sweep voltammetry (LSV) measurements were performed in 0.1 M KCl containing 5 mM potassium ferrocyanide $(K_4[Fe(CN)_6])$ to evaluate the electrochemical behaviour of the IMS and IMS-MOF catalysts (Figure 7).

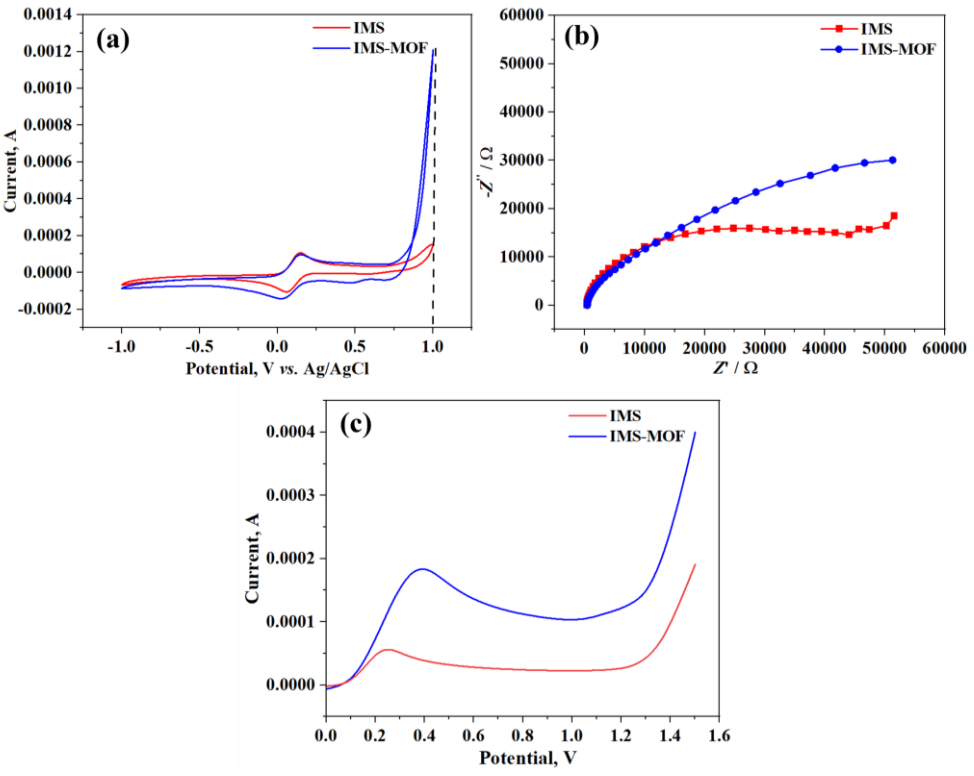


Figure 6. Electrochemical characterization of IMS and IMS-MOF catalysts: (a) cyclic voltammetry (CV) curves recorded in 0.1 M KCl containing 5 mM K_4 [Fe(CN)₆] at a scan rate of 0.5 V s⁻¹, (b) EIS Nyquist plots obtained in the same electrolyte, recorded over a frequency range of 0.1 to 100 kHz with an AC perturbation amplitude of 5 mV, (c) Linear sweep voltammetry (LSV) profiles measured under light illumination in the same electrolyte at a scan rate of 0.5 V s⁻¹

The CV profile of IMS-MOF is displayed in Figure 7a, showing higher current response than that of IMS, indicating better redox properties and superior electron transfer capability [47]. Instead, the incorporation of the BTC linker in between the IMS-MOF framework generates the π -conjugated electron pathways, thus assisting in enhancing charge mobility and electron transfer of redox reaction [47]. The broader peak separation in the CV of IMS indicates a slower electron transfer kinetics [48]. This is probably due to the lack of orderly conductive networks introduced through the MOF structure in IMS-MOF. In contrast, the aromatic backbone structure of the BTC linker is beneficial for electron delocalization, which can efficiently decrease the electron hopping resistance and further promote the redox property of IMS-MOF. Especially, the CV exhibited analogous redox processes of IMS-MOF and Fe-Ni LDH@ZIF-67/CC composite, suggesting equivalent electrochemical activity [49].

Based on Figure 7b, electrochemical impedance spectroscopy (EIS) was used to examine the charge transfer and ion diffusion behaviour of the IMS and IMS-MOF catalysts. The Nyquist plots for both samples display a linear region at low frequencies, which is mainly influenced by Warburg impedance, indicating that ion diffusion is the dominant process in this region [50]. This linear trend reflects diffusion-controlled behaviour, while charge transfer resistance typically appears as a semicircular arc at higher frequencies. The steeper slope observed for IMS compared to IMS-MOF suggests that ions diffuse more easily within the IMS structure, likely due to its simpler framework [20]. However, despite showing faster ion diffusion, IMS suffers from long-term instability caused by metal leaching, which can reduce its overall performance over time. Although the Nyquist plot for IMS-MOF shows a slightly less steep line, indicating that ion diffusion is somewhat more restricted within the structure, the presence of the BTC linker plays an essential role in enhancing the material's stability. The BTC linker improves electron transport and reduces metal leaching, contributing to better structural integrity [51,52]. These advantages compensate for minor diffusion limitations related to IMS-MOF. This is due to the well-ordered porous network offered by a MOF structure of the BTC linker [25]. This network could impose some restrictions on the movement of ions compared with IMS; however, it greatly increases the overall electron transfer ability and long-term stability of the material [53]. The semicircle radius in the Nyquist plot of IMS-MOF was smaller than that of IMS, showing a lower charge transfer resistance and better interfacial conductivity. Such enhancement is attributed to the electron delocalization mediated by Fe-O-C bonding, thus forming a stable path for electron transition in the framework [20]. Meanwhile, the current responses for IMS-MOF in cyclic voltammetry (CV) measurement were higher as well, also reflecting its stronger redox activity and more stable Fe²⁺/Fe³⁺ recycling [29]. Interestingly, even though IMS showed a relatively higher ion diffusion rate, its fast Fe leaching led to unstable redox cycling and unsatisfactory long-term activity. On the other hand, the BTC linker has structural restrictions that secure the Fe active sites, making a more sturdy and effective electron transfer environment. This stabilization not only eliminates charge recombination but also reduces the loss of metal ions in recycling [54]. Therefore, IMS-MOF achieves sufficient ion migration with greatly enhanced electronic conductivity and structure stability as well as being a superior catalyst for long-lasting photocatalytic effects.

In general, LSV was conducted under light illumination to examine the photoelectrochemical performance of IMS and IMS-MOF (Figure 7c). Both materials exhibited an increase in current density with increasing potential, indicating enhanced electrochemical activity [45]. However, the dominant processes contributing to the current response vary across the potential range. At potentials below 1.0 V, the current response is mainly influenced by photoelectrochemical processes, as light absorption promotes charge separation and electron transfer within the catalyst [55]. The presence of the BTC linker in the IMS-MOF framework plays a key role in enhancing these processes by reducing the

band gap energy and improving light absorption, which facilitates more efficient charge transfer. In contrast, at potentials above 1.0 V, the response is primarily governed by electrochemical water oxidation, where the influence of photoirradiation becomes less significant [56].

Furthermore, the linear sweep voltammetry (LSV) measurements exhibit much higher catalytic current densities for IMS-MOF than those of IMS, indicating a higher catalytic intrinsic redox capacity. This enhancement could be ascribed to the bimetallic nature of the system, where the Fe centres actively mediate the Fe³+/Fe²+ redox. The BTC linker is sectioned with nontopological positions covalently incorporated into its framework, remaining a rigid backbone that stabilizes metal sites and facilitates efficient electron delocalization [57]. The existence of such an extended Fe-O-C network guarantees fast electron transport and eliminates charge recombination, accordingly enabling IMS-MOF to achieve high current densities even at low light input, for instance, in water electrolysis [58]. This dual role of Fe redox activity and structural/electronic stabilization provided by BTC further demonstrates the enhanced versatility of IMS-MOF compared to pristine-IMS. Collectively, the electrochemical analyses (EIS, CV and LSV) demonstrate that the inherent natures of IMS-MOF, such as reduced band gap energy, enhanced charge transfer ability and intensified redox activity, are attributed to synergistic interaction between metal coordination centres and organic ligands behind its excellent photocatalytic performance.

Methylene blue removal mechanism

Effect of catalyst loading

This study aimed to examine the effectiveness of both IMS and IMS-MOF catalysts for the removal of methylene blue (MB) from aqueous solutions, emphasizing the effects of catalyst loadings and metal leaching, which occurred simultaneously (Figure 8a). Increasing the IMS catalyst loading leads to a near-quantitative MB removal efficiency.

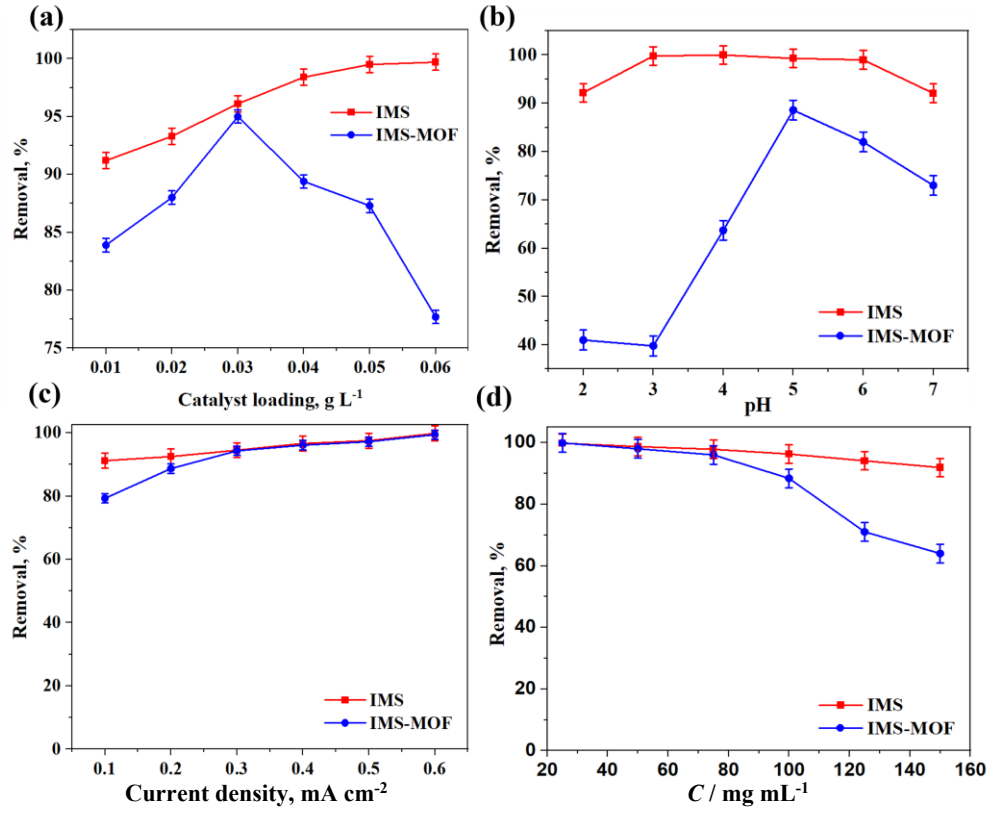


Figure 7. Photoelectrochemical degradation of MB at different (a) catalyst loadings, (b) pH, (c) current densities, (d) MB initial concentrations

However, this apparent performance enhancement was, at least partially, attributable to metal leaching, where dissolved metal ions contributed to MB degradation. This process is unsustainable and raises significant environmental concerns due to potential secondary contamination. The IMS-MOF catalyst exhibited a maximum methylene blue removal efficiency of approximately 95 % at an optimal loading of 0.03 g L⁻¹. The observed trend suggests that catalyst concentration plays a crucial role in the photoelectrochemical degradation process. At lower dosages, the limited number of active sites restricts the generation of reactive species, thereby reducing efficiency. Increasing the loading up to 0.03 g L⁻¹ enhances light absorption and provides sufficient surface-active sites, resulting in superior performance. However, further increase beyond this concentration led to a decline in removal efficiency, which can be attributed to excessive turbidity, reduced light penetration, and mass transfer resistance rather than catalyst instability. Importantly, the MOF modification minimized metal leaching, confirming that the reduced activity at higher dosages is governed by intrinsic process limitations rather than material degradation. This emphasizes the efficiency of the preservative action of the MOF structure through the stabilization of the active catalytic sites against the leaching of controlled metallic ions into the solution [51]. As a result, the IMS-MOF catalyst provides a greener and more sustainable route for MB treatments compared to the unmodified IMS catalyst.

Effect of pH

All the obtained data regarding MB removal as a function of initial pH ranging from 2 to 7 for both IMS and IMS-MOF catalysts are exhibited in Figure 8b. The IMS catalyst showed pH-independent behaviour with high MB removal efficiencies. Nonetheless, the observed independence of pH is further complicated by the contributions of metal leaching, which is enhanced at acidic conditions [59]. At pH 5, MB removal reached 90 %, indicating excellent performance of the IMS-MOF catalyst. The pH-dependent behaviour reflects the inherent stability of the MOF framework, effectively limiting the leaching of metals while demonstrating considerable catalytic activity at a near-neutral pH [40]. The high MB removal efficiency of the IMS catalyst is deceptive since metal leaching, especially in acidic media, is a significant source of MB degradation. On the other hand, the result of the IMS-MOF catalyst more closely approximates its inherent catalytic activity since its metallic species is embedded within a MOF structure capable of preventing metal leaching under the tested pH conditions [60]. The structural stability is indicative of the stability of the IMS-MOF catalyst, as well as the minimum loss of metal and the fact that the result provides a more accurate measure of the overall catalytic activity.

Effect of current density

The effect of applied current density on MB removal was investigated for both IMS and IMS-MOF catalysts, as shown in Figure 8c. The MB removals for both IMS and IMS-MOF catalysts increased with higher current density, nearly reaching 100 % removal at a higher current density. Importantly, the performance gap between the two catalysts narrowed at high current densities. The agreement in performance at higher current densities is likely because of the impact of the electrochemical environment. In this scenario, the metal leaching contribution to MB degradation is minimized, allowing the intrinsic catalytic activity of the IMS-MOF catalyst to be better evaluated [61,62]. The stable design of the IMS-MOF catalyst affords efficient activity without the tandem environmental risks of metal leaching, which is highly pertinent for the IMS catalyst. As such, at higher current densities, the intrinsic benefits of the IMS-MOF catalyst, specifically its shelf stability and diminished leaching, become more pronounced.

Effect of methylene blue concentration

The influence of initial MB concentration on the performance of IMS and IMS-MOF catalysts was also investigated in Figure 8d. The IMS catalyst maintained relatively high MB removal efficiency even at elevated initial MB concentrations. However, this sustained performance is, at least in part, attributable to the continuous release of metal ions from the catalyst, which contributes to MB degradation. In contrast, the IMS-MOF catalyst exhibited a decrease in MB removal efficiency with increasing initial MB concentration. This behaviour is consistent with the absence of significant metal leaching, as the degradation process relies solely on the availability of active catalytic sites within the MOF structure [63]. While the IMS catalyst appears to demonstrate superior performance at high MB concentrations, this apparent advantage is a consequence of undesirable metal leaching.

The superior photocatalytic performance of IMS-MOF is attributed to the synergistic effect between Fe metal centres and BTC organic ligands. Fe sites are the major redox-active centres that can be converted between Fe^{2+} and Fe^{3+} to promote Fenton-like reactions for sustained ROS production [63]. On the other hand, an elongated π -conjugation system in the BTC linker and electron-donating carboxylate groups helps for electronic charge spreading, leading to lower C-H recombination [64]. This synergetic interaction decreases the band gap, enhances visible light absorption and promotes the interface charge transfer. Thus, the metal-ligand system exhibits better photocatalytic activity and stability than either component alone, as the ligand stabilizes Fe centres while the metal contributes to redox activity that is otherwise not possible from the ligand.

Reusability studies

The reusability and long-term stability of these IMS and IMS-MOF catalysts are crucial factors for establishing their practical application in dye degradation. As shown in Figure 9, both the catalysts suffered an activity drop during repeated recycling. Nevertheless, the degree of deactivation differed significantly in the two systems. In the case of IMS, the degradation efficiency fell dramatically by approximately 81 % after ten cycles, revealing a poor durability for continuous operation. Conversely, IMS-MOFs showed significantly improved stability and a slight 15.1 % activity drop, which verified the promoting effects of MOF loading on the catalysis.

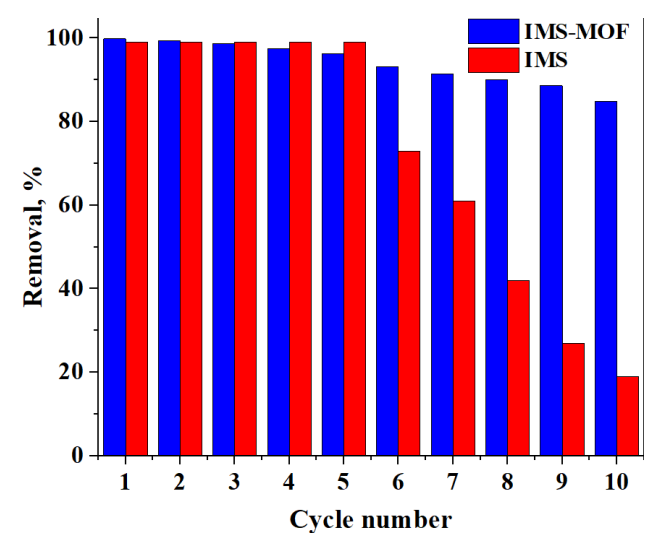


Figure 8. Reusability of IMS and IMS-MOF for MB removal (reaction conditions: catalyst loading 0.01 g L^{-1} , $C_{MB} = 50$ mg L^{-1} , pH 5, current density 1 mA cm⁻²)

Higher stability of IMS-MOF could result from stronger coordination of the Fe centre by the BTC linker, which stabilizes the Fe active sites to prevent metal leaching. This is further confirmed by ICP-

OES data, which showed very low Fe ion release for IMS-MOF (0.032 ppm) when the MOF was recycled, compared to the substantial release of Fe ions from IMS (16.7 ppm). Thus, the inhibition of Fe dissolution is the dominant reason for the improved reusability of IMS-MOF.

In addition to metal leaching, other deactivation routes also played a role in the deterioration of catalytic performance. Deposition of reaction intermediates and/or mineralization-resistant side products can also coat the surface area, block active sites and slow down interfacial charge transfer, hence decreasing the rate of dye removal. Not directly probed, but potential damage to the catalyst lattice, meaning potentially partial collapse of the MOF or loss of crystallinity during multiple irradiation and redox cycling, can work against performance over long usage. Moreover, stability restrictions have been observed in other MOF and Fe-based photocatalysts due to degradation of the structure, fouling of the surface and leaching, collectively controlling their long-term applicability [65]. Collectively, these results underscore that while its activity significantly stabilizes towards IMS, strategies to prevent surface deactivation and preserve structural integrity remain necessary after long-term operations and should be the focus of future studies.

Coordinated by the Fe sites, BTC forms a robust and narrowly distributed array that can prevent fast dissolution of Fe species and sustain catalytic cycling over several cycles. In addition to the strengthening effect of the structure, π -conjugated aromatic rings and electron-donating carbo-xylate groups in BTC can induce spatial delocalization of electrons, which is beneficial for increasing electron transfer between adjacent domains as well as prolonging e^-/h^+ pair lifetimes [66]. This multifunction not only leads to the limited band gap of IMS-MOF, but it also benefits the ROS generation through inducing electron transfer to O_2 and H_2O_2 . As a result, the BTC ligand is essential for the synergistic effect of structural stability and enhanced photocatalytic activity that makes IMS-MOF different from unstable pristine IMS.

Scavenging experiment

To shed light on the photocatalytic degradation of methylene blue (MB) using the synthesized IMS-MOF catalyst, a thorough analysis of its electronic properties and the reactive oxygen species (ROS) involved was performed. The UV-visible spectroscopy was conducted in a solid state to estimate the band gap energy (Eg), a crucial factor influencing the material's light absorption properties. The energy gap between the highest occupied molecular orbital (HOMO) and the lowest unoccupied molecular orbital (LUMO) determines the photo-response of the material [67]. Photoabsorption occurs when the energy of the incident photon is equal to or higher than Eg, and it excites the electrons from the valence band (VB) to the conduction band (CB), generating electronhole (e⁻/h⁺) pairs. Scavenging experiments were also performed with selective quenchers to investigate the key ROS produced in the MB degradation. The AgNO₃, hydrogen peroxide (H₂O₂), pbenzoguinone (PBQ), and ethylenediaminetetraacetic acid disodium salt (EDTA-2Na) were used as the scavengers of electrons (e⁻), hydroxyl radicals (\cdot OH), superoxide anion radicals (\cdot O₂⁻), and photogenerated holes (h⁺), respectively. The data showed minimal effect on the MB degradation efficiency after the induction of EDTA-2Na and AgNO₃, Figure 10. On the other hand, a significant (45 %) decrease in degradation was observed upon addition of PBQ, suggesting an essential contribution of ·O₂⁻ as a major active species. Furthermore, the significant inhibitory effect of H₂O₂ on dye degradation underscores the critical involvement of both \cdot OH and \cdot O₂⁻ radicals in the degradation process.

Based on these results and considering the analysis of electronic properties for the iron-based catalyst, a plausible mechanism for photocatalytic degradation is proposed in Figure 11. X-ray spectroscopy (XPS) indicated coexistence of Fe²⁺ and Fe³⁺ oxidation states in the catalyst structure,

which is critical for redox cycles during photocatalysis. The narrow band gap of IMS-MOF allows an effective absorption of photons, which is beneficial for the excitation of electrons from the VB to CB and forming electron-hole (e^-/h^+) pairs [68]. The photogenerated holes (h^+) are characterized with strong oxidative ability, which can directly oxidize the adsorbed H₂O molecules to produce hydroxyl radicals (·OH), and the CB electrons ultimately reduce the dissolved O₂ to generate superoxide radicals (·O²⁻) [68].

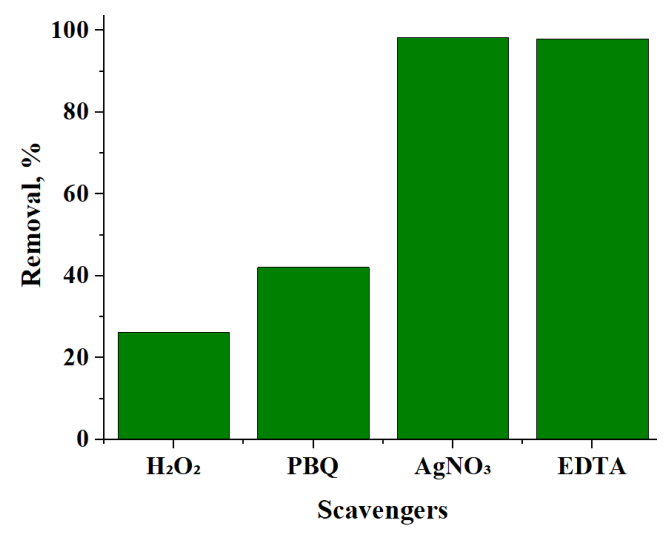


Figure 9. Different quencher effects of the IMS-MOF catalyst for MB removal

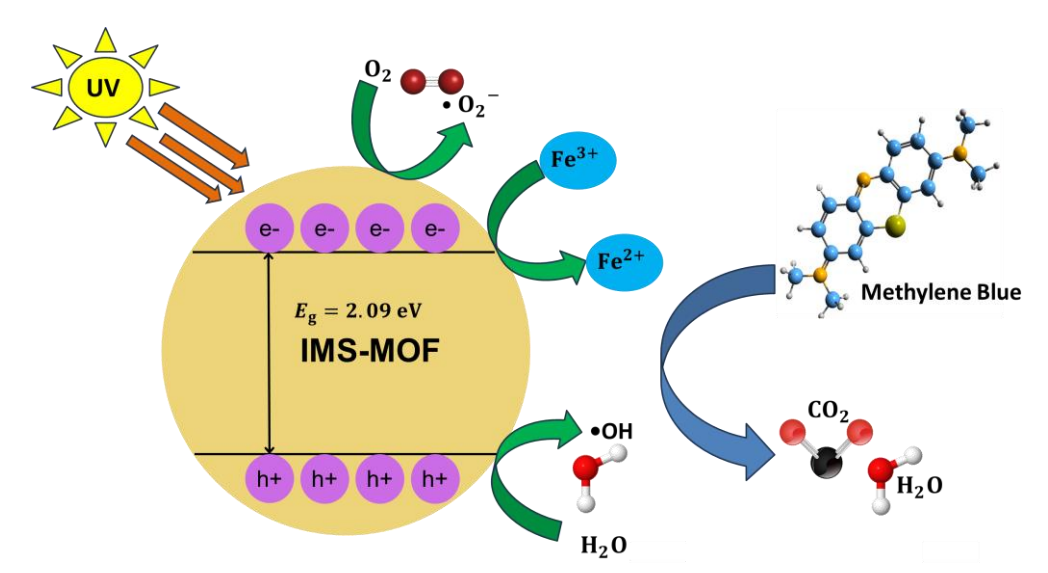


Figure 10. Schematic of the MB removal by IMS-MOF through photoelectrochemical reactions

The CB electron potential of IMS-MOF is above the redox potential of Fe^{3+}/Fe^{2+} in water, allowing Fe^{3+} species to serve as electron traps and suppress fast e-counter-arrow recombination. In this oxidation, Fe^{3+} is reduced to Fe^{2+} , and the reduced form of iron (Fe^{2+}) reacts with H_2O_2 via a Fenton-like reaction to generate ·OH radicals (Equations (2) to (4)). At the same time, dissolved O_2 molecules are reduced by CB electrons to form O_2 radicals (Equation (6)), which can further react to yield additional reactive oxygen species (ROS), such as ·OH and H_2O_2 . These combined processes enhance the oxidative capability of the system [69].

In addition, the photosensitization effect of methylene blue (MB) contributes to the degradation pathway. Under light irradiation, MB molecules absorb photons and are excited into MB* (singlet or triplet states) (Equation (2)). The excited MB* species can then donate electrons to O_2 , generating O_2 radicals (Equation (8)), or transfer electrons to H_2O_2 to produce OH radicals. This dual role of MB, as

both a target pollutant and a photosensitizer, significantly promotes ROS formation and accelerates dye degradation (Equation (9)). Similar photosensitization-assisted Fenton-like mechanisms have been reported for iron complexes with carboxylic acid ligands, supporting the proposed mechanism in this work [29].

These findings further confirm that both photosensitization and ROS generation play crucial roles in MB degradation. The formation of $\cdot O_2^-$ is facilitated by the reduction of molecular O_2 via CB electrons, while H_2O_2 is a key precursor for ROS generation under photoelectrochemical conditions, producing both superoxide and hydroxyl radicals. These ROS act as the main oxidizing agents responsible for the breakdown of organic dye molecules, following a sequence of redox reactions as outlined in Equations (2) to (9) [29].

MB + IMS catalysts +
$$hv \rightarrow$$
 IMS catalysts $h^{+} + e^{-}$ MB*

(2)

 $Fe^{3^{+}} + H_{2}O_{2} \rightarrow \cdot O_{2}H + Fe^{2^{+}} + h^{+}$

(3)

 $Fe^{2^{+}} + H_{2}O_{2} \rightarrow Fe^{3^{+}} + \cdot OH + OH^{-}$

(4)

 $Fe^{3^{+}} + e^{-} \rightarrow Fe^{2^{+}}$

(5)

 $e^{-} + O_{2} \rightarrow \cdot O_{2}^{-}$

(6)

 $h^{+} + OH^{-} + H_{2}O \rightarrow \cdot OH$

(7)

 $MB^{*} + H_{2}O_{2} + O_{2} \rightarrow \cdot OH + \cdot O_{2}^{-}$

(8)

The enhanced photocatalytic activity of IMS-MOF arises from the strong synergy between Fe centres and BTC linkers, which modifies its electronic structure and narrows the band gap. This allows IMS-MOF to absorb visible light more effectively, exciting electrons from the valence band (VB) to the conduction band (CB) and leaving behind holes in the VB. The efficient separation of these charge carriers, supported by EIS and CV analyses, minimizes recombination and promotes the formation of reactive oxygen species (ROS), such as superoxide ($-O_2$ ·) and hydroxyl radicals (\cdot OH). These ROS actively degrade methylene blue into intermediates and ultimately into CO₂ and H₂O.

In comparison, unmodified IMS, with its wider band gap and poorer charge transport, shows almost no visible-light activity. As summarized in Figure 11, the dual coordination of BTC-Fe not only narrows the band gap but also enhances charge migration and ROS generation, explaining the significant improvement in IMS-MOF's photocatalytic performance.

Conclusions

 \cdot OH + \cdot O₂⁻ + MB* \rightarrow Degraded products

The synthesized IMS-MOF demonstrated strong potential for removing methylene blue from textile wastewater, achieving degradation efficiencies above 90 %. The removal mechanism followed a typical photocatalytic pathway characterized by effective charge separation and enhanced photocatalytic activity. IMS-MOF also exhibited excellent stability across a wide pH range and maintained its performance well in the presence of common co-existing ions. The improved degradation efficiency can be mainly attributed to the oxidative radicals generated through the in-situ formation of hydrogen peroxide (H_2O_2). Furthermore, by minimizing the release or dissolution of metal ions, the surface modification ensures long-term applicability through reduced metal leaching. The material's stability and reusability were confirmed through successive degradation cycles. Given the large volumes of dye-contaminated effluents produced by the textile industry, this study presents a novel and eco-friendly strategy for sustainable wastewater remediation. Future work should focus on optimizing the adsorption capacity and mechanical stability of the material, as well as expanding its applicability to a broader range of organic pollutants in industrial wastewater.

(9)

References

- [1] Y. Jiang, C. Fu, B. Xu, J. Cui, Y. Feng, L. Tan, Performance of a novel Built-in Static Magnetic Field Biological Aerated Filter (BSMF-BAF) for treating high-salt textile dyeing wastewater, *Journal of Environmental Management* **370** (2024) 122548. https://doi.org/10.1016/j.jenvman.2024.122548
- [2] M. Sanavi Fard, A. Ehsani, F. Soleimani, Treatment of synthetic textile wastewater containing Acid Red 182 by electro-Peroxone process using RSM, *Journal of Environmental Management* **344** (2023) 118379. https://doi.org/10.1016/j.jenvman.2023.118379
- [3] J. Hassan, M. Tariq, N. Anwar, M. U. Farid, F. Hussain, H. Rasheed, Assessment of heavy metals accumulation by vegetables irrigated with different stages of textile wastewater for evaluation of food and health risk, *Journal of Environmental Management* **353** (2024) 120206. https://doi.org/10.1016/j.jenvman.2024.120206
- [4] E. Bustos, Textile-washing wastewater treatment using ozonolysis, electro-coagulation, and electro-oxidation, *Electrochimica Acta* **512** (2025) 146599. https://doi.org/10.1016/j.electacta.2024.145473
- [5] M. Tabish, A. B. Tabinda, Z. Mazhar, A. Yasar, J. Ansar, I. Wasif, Physical, chemical and biological treatment of textile wastewater for removal of dyes and heavy metals, Desalination and Water Treatment 320 (2024) 100842. https://doi.org/10.1016/j.dwt.2024.100842
- [6] I. Ghosh, S. Kar, T. Chatterjee, N. Bar, S. K. Das. Removal of methylene blue from aqueous solution using *Lathyrus sativus* husk: Adsorption study, MPR and ANN modelling, *Process Safety and Environmental Protection* 149 (2021) 345-361. https://doi.org/10.1016/j.psep.2020.11.003
- [7] L. Miao, Z. Liu, J. Zhang, C. Wang, Y. Wang, S. Chen, Sustainable reuse of nickel converter slag as a heterogeneous electro-fenton catalyst for treating textile dyeing wastewater: Activity, mechanism and stability assessment, *Journal of Cleaner Production* **378** (2022) 134421. https://doi.org/10.1016/j.jclepro.2022.134421
- [8] F. C. Ardiati, R. M. Nugraha, A. R. Putra, H. S. Kurniawan, M. P. Saputra, D. D. Tjahjono. Evaluation of batch and fed-batch rotating drum biological contactor using immobilized *Trametes hirsuta* EDN082 for non-sterile real textile wastewater treatment, *Journal of Environmental Chemical Engineering* 12 (2024) 113241. https://doi.org/10.1016/j.jece.2024.113241
- [9] M. F. Majnis, M. A. Mohd Adnan, S. P. Yeap, N. Muhd Julkapli, How can heteroatoms boost the performance of photoactive nanomaterials for wastewater purification?, *Journal of Environmental Management* 366 (2024) 121808. https://doi.org/10.1016/j.jenvman.2024.121808
- [10] N. Ardhan, P. Tongpadungrod, C. Phalakornkule, Effects of auxiliary chemicals and dye solubility on chemical oxygen demand reduction of dyes by electrocoagulation with Fe electrode, *Materials Today: Proceedings* **52** (2021) 2529-2533. https://doi.org/10.1016/j.matpr.2021.10.446
- [11] Y. Ran, R. Cui, X. Wang, H. Wang, L. Zhang, L. Xu, Advancements in iron-based photocatalytic degradation for antibiotics and dyes, *Journal of Environmental Management* **374** (2025) 123991. https://doi.org/10.1016/j.jenvman.2024.123991
- [12] E. Issaka, M. Adams, S. El-Ouardy, J. Baffoe, M. Enyan, N. A. Johnson. Photoelectrochemical alchemy: Transforming wastewater pollutants through photoelectrochemical advanced oxidation processes, *Desaline and Water Treatment* 321 (2024) 101057. https://doi.org/10.1016/j.dwt.2025.101057
- [13] N. A. Sacco, F. A. Marchesini, I. Gamba, G. García. Photoelectrochemical Degradation of Contaminants of Emerging Concern with Special Attention on the Removal of



- Acetaminophen in Water-Based Solutions, *Catalysts* **13** (2023) 13030524. https://doi.org/10.3390/catal13030524
- [14] Q. Dang, W. Zhang, J. Liu, L. Wang, D. Wu, D. Wang, Bias-free driven ion assisted photoelectrochemical system for sustainable wastewater treatment, *Nature Communications* **14** (2023) 8413. https://doi.org/10.1038/s41467-023-44155-5
- [15] B. Sarkodie, L. Luo, Z. Mao, A. Farooq, Q. Feng, C. Xu, B. Tawiah, Y. Hu, Highly reusable Bi₂O₃/electron-Cu-shuttle in-situ immobilized polyacrylonitrile fibrous mat for efficient photocatalytic degradation of methylene blue and rhodamine B dyes, *Journal of Environmental Management* **354** (2024) 120346. https://doi.org/10.1016/j.jenvman.2024.120346
- [16] R. Koutavarapu. ZnO nanosheets-decorated Bi₂WO₆ nanolayers as efficient photocatalysts for the removal of toxic environmental pollutants and photoelectrochemical solar water oxidation, *Journal of Environmental Management* **265** (2020) 110504. https://doi.org/10.1016/j.jenvman.2020.110504
- [17] F. Cheng, S. Guo, Z. Cheng. Stabilization of arsenic-cadmium co-contaminated soil with the iron-manganese sludge derived amendment: Effects and mechanisms, *Journal of Environmental Management* **370** (2024) 122570. https://doi.org/10.1016/j.jenvman.2024.122570
- [18] J. Vaz-Ramos, S. Le Calvé, S. Begin, Polycyclic aromatic hydrocarbons in water environments: Impact, legislation, depollution processes and challenges, and magnetic iron oxide/graphene-based nanocomposites as promising adsorbent solutions, *Journal of Hazardous Materials* **490** (2025) 137726. https://doi.org/10.1016/j.jhazmat.2025.137726
- [19] S. Hegazy, H. H. Ibrahim, T. Weckman, T. Hu, S. Tuomikoski, U. Lassi, K. Honkala, V. Srivastava, Synergistic pyrolysis of Cellulose/Fe-MOF Composite: A Combined experimental and DFT study on dye removal, *Chemical Engineering Journal* **504** (2024) 158654. https://doi.org/10.1016/j.cej.2024.158654
- [20] R. Vijayarangan, K. Gayathri, S. Mohan, R. Ilangovan, I. A. Ahmed, Influence of ligands in Fe-MOFs on deriving iron oxide (α-Fe₂O₃) nanostructures for enhanced photocatalytic degradation and water splitting reactions, *Surfaces and Interfaces* 56 (2025) 105726. https://doi.org/10.1016/j.surfin.2024.105726
- [21] Z. Gao, B. Deng, L. Xu, K. Du, Enhanced removal of organic dyes by piezoelectric-Fenton-like treatment with Fe-MOF@MoS₂ catalysts, *Journal of Alloys and Compounds* **1007** (2024) 176474. https://doi.org/10.1016/j.jallcom.2024.176474
- [22] Z. Wang, S. Zhu, J. Deng, H. Li, L. Wang, H. Luo, Z. Tang, X. Li, Facile Preparation of Fe₃O₄@SiO₂ Derived from Iron-Rich Sludge as Magnetic Catalyst for the Degradation of Organic Contaminants by Peroxymonosulfate Activation, *Sustainability* **14** (2022) 142416419. https://doi.org/10.3390/su142416419
- [23] G. de V. Brião, T. B. da Costa, R. Antonelli, J. M. Costa, Electrochemical processes for the treatment of contaminant-rich wastewater: A comprehensive review, *Chemosphere* **355** (2024) 141884. https://doi.org/10.1016/j.chemosphere.2024.141884
- [24] F. Li, G. Wang, J. Ren, C. Sun. Synthesis Methods and Influencing Factors of Metal Organic Framework Material MIL-53, *Journal of Physics: Conference Series* **2194** (2022) 012030. https://doi.org/10.1088/1742-6596/2194/1/012030
- [25] X. Liu, Y. Shan, S. Zhang, Q. Kong, H. Pang, Application of metal organic framework in wastewater treatment, *Green Energy and Environment* **8** (2022) 698-721. https://doi.org/10.1016/j.gee.2022.03.005
- [26] A. Wang, K. Barcus, S. M. Cohen, Quantifying Ligand Binding to the Surface of Metal-Organic Frameworks, *Journal of American Chemical Society* **145** (2023) 16821-16827. https://doi.org/10.1021/jacs.3c04892

- [27] J. Jangra, S. Singh, J. Shah, and R. K. Kotnala, Green electricity production through iron oxide and Fe-MOF composite based hydroelectric cell, *Applied Materials Today* **43** (2025) 102652. https://doi.org/10.1016/j.apmt.2025.102652
- [28] P. Dinh Du, P. Ngoc Hoai, Synthesis of MIL-53(Fe) Metal-Organic Framework Material and Its Application as a Catalyst for Fenton-Type Oxidation of Organic Pollutants, *Advances in Materials Science and Engineering* **2021** (2021) 5540344. https://doi.org/10.1155/2021/5540344
- [29] H. Chen, Iron complexes synthesized from FeOCI with carboxylic acid based ligands as Fenton-like catalysts for the highly efficient degradation of organic dyes over a wide pH range, Colloids and Surfaces A Physicochemical and Engineering Aspects **705** (2025) 135697. https://doi.org/10.1016/j.colsurfa.2024.135697
- [30] P. Goyal, C. S. Tiwary, S. K. Misra, Ion exchange based approach for rapid and selective Pb(II) removal using iron oxide decorated metal organic framework hybrid, *Journal of Environmental Management* **277** (2021) 111469. https://doi.org/10.1016/j.jenvman.2020.111469
- [31] L. Yang, L. Bi, X. Tao, L. Shi, P. Li, Highly efficient removal of tetracyclines from water by a superelastic MOF-based aerogel: Mechanism quantitative analysis and dynamic adsorption, *Journal of Environmental Management* **353** (2024) 120169. https://doi.org/10.1016/j.jenvman.2024.120169
- [32] F. Zou, R. Yu, R. Li, W. Li, Microwave-assisted synthesis of HKUST-1 and functionalized HKUST-1-@H₃PW₁₂O₄₀: Selective adsorption of heavy metal ions in water analyzed with synchrotron radiation, *ChemPhysChem* **14** (2013) 2825-2832. https://doi.org/10.1002/cphc.201300215
- [33] A. E. J. Hoffman, W. Temmerman, E. Campbell, A. A. Damin, I. Lezcano-Gonzalez, A. M. Beale, A Critical Assessment on Calculating Vibrational Spectra in Nanostructured Materials, *Journal of Chemical Theory and Computation* **20** (2024) 513-531. https://doi.org/10.1021/acs.jctc.3c00942
- [34] M. V. Solovyeva, A. I. Shkatulov, L. G. Gordeeva, E. A. Fedorova, T. A. Krieger, Y. I. Aristov, Water Vapor Adsorption on CAU-10- X: Effect of Functional Groups on Adsorption Equilibrium and Mechanisms, *Langmuir* **37** (2021) 693-7029. https://doi.org/10.1021/acs.langmuir.0c02729
- [35] K. I. Hadjiivanov, D. A. Panayotov, M. Y. Mihaylov, E. Z. Ivanova, K. K. Chakarova, S. M. Andonova, Power of Infrared and Raman Spectroscopies to Characterize Metal-Organic Frameworks and Investigate Their Interaction with Guest Molecules, *Chemical Reviews* **121** (2021) 1286-1424. https://doi.org/10.1021/acs.chemrev.0c00487
- [36] J. N. Jocz, Y. Lyu, B. J. Hare, C. Sievers, Characterization of Surface Species during Benzene Hydroxylation over a NiO-Ceria-Zirconia Catalyst, *Langmuir* **38** (2022) 458-471. https://doi.org/10.1021/acs.langmuir.1c02833
- [37] A. Amari, H. Gannouni, M. I. Khan, M. K. Almesfer, A. M. Elkhaleefa, A. Gannouni, Effect of structure and chemical activation on the adsorption properties of green clay minerals for the removal of cationic dye, *Applied Science* **8** (2018) 8112302. https://doi.org/10.3390/app8112302
- [38] H. R. Abid, M. R. Azhar, S. Iglauer, Z. H. Rada, A. Al-Yaseri, A. Keshavarz, Physicochemical characterization of metal organic framework materials: A mini review, *Heliyon* **10** (2024) e23840. https://doi.org/10.1016/j.heliyon.2023.e23840
- [39] I. Bechis, A. F. Sapnik, A. Tarzia, E. H. Wolpert, M. A. Addicoat, D. A. Keen, T. D. Bennett, K. E. Jelfs, Modeling the Effect of Defects and Disorder in Amorphous Metal-Organic Frameworks, Chemistry of Materials 34 (2022) 9042-9054. https://doi.org/10.1021/acs.chemmater.2c01528



- [40] Z. Zhao, S. Li, Y. Zhang, P. Guo, X. Zhao, Y. Li, Repurposing of steel rolling sludge: Solvent-free preparation of α-Fe₂O₃ nanoparticles and its application for As(III/V)-containing wastewater treatment, *Journal of Environmental Management* **342** (2023) 118286. https://doi.org/10.1016/j.jenvman.2023.118286
- [41] X. Huang, K. Wu, F. Yang, R. Fu, Redox photocatalysis CuFe-BTC for nitrate reduction and formaldehyde oxidation, *Chemical Engineering Journal* **504** (2025) 158995. https://doi.org/10.1016/j.cej.2024.158995
- [42] J. Cao, G. Tang, F. Yan, Applications of Emerging Metal and Covalent Organic Frameworks in Perovskite Photovoltaics: Materials and Devices, *Advanced Energy Materials* **14** (2024) 202304027. https://doi.org/10.1002/aenm.202304027
- [43] R. Bashiri, P. S. Lawson, S. He, S. Nanayakkara, K. Kim, N. S. Barnett, Discovery of Dual Ion-Electron Conductivity of Metal-Organic Frameworks *via* Machine Learning-Guided Experimentation, *Chemistry of Materials* **37** (2025) 1143-1153. https://doi.org/10.1021/acs.chemmater.4c02974
- [44] X. Huang, W. Ye, J. Zhuang, C. Hu. π-Conjugated Structure Enhances the UV Absorption Performance of Carbon Dots and Application in the Design of Light-Colored Sunglasses, *ACS Sustainable Chemistry & Engineering* **12** (2024) 10399-10410. https://doi.org/10.1021/acssuschemeng.4c01739
- [45] H. B. Albargi, A. Abbas, M. Zeeshan, M. W. Iqbal, N. A. Ismayilova, Design of iron-based metal-organic framework (Fe-MOF) and molybdenum telluride (MoTe₂) nanohybrids for enhanced energy storage and hydrogen evolution reactions, *Inorganic Chemistry Communications* **173** (2025) 113791. https://doi.org/10.1016/j.inoche.2024.113791
- [46] M. Priyadarshini, A. Ahmad, M. M. Ghangrekar, Efficient upcycling of iron scrap and waste polyethylene terephthalate plastic into Fe₃O₄@C incorporated MIL-53(Fe) as a novel electro-Fenton catalyst for the degradation of salicylic acid, *Environmental Pollution* **322** (2023) 121242. https://doi.org/10.1016/j.envpol.2023.121242
- [47] H. E. Emam, T. Koto, K. Sebőkné Nagy, M. El-Shahat, H. Abdel-Gawad, Synthesis, spectroscopic study and carbofuran adsorption of mixed metal (Co, Cu)@Ca-BTC frameworks aimed at wastewater cleaning, *Journal of Industrial and Engineering Chemistry* **139** (2024) 444-457. https://doi.org/10.1016/j.jiec.2024.05.019
- [48] J. Park, G. Lee, W-G Lim, T-N Kim, C-Y Yoo, S. Yu, J. Yoon, J. Chun, J. Hwang, Direct hybridization of Fe-MOF and polymer to fabricate iron oxide/carbon nanorod microsphere anodes for lithium-ion batteries, *Applied Surface Science* **682** (2025) 161756. https://doi.org/10.1016/j.apsusc.2024.161756
- [49] S. Cheng, B. Wu, Y. Pang, X. Shen, Highly efficient heterogeneous electro-Fenton reaction for tetracycline degradation by Fe-Ni LDH@ZIF-67 modified carbon cloth cathode: Mechanism and toxicity assessment, *Journal of Environmental Management* **354** (2024) 120336. https://doi.org/10.1016/j.jenvman.2024.120336
- [50] D. Mishra, S. S. Jamuar, A. Krause, S. Chatterjee, Iron terephthalate MOF-MWCNTs based composite paste two-electrode system for selective detection of lead in contaminated stream, *Journal of Environmental Chemical Engineering* 12 (2024) 113561. https://doi.org/10.1016/j.jece.2024.113561
- [51] A. M. P. Peedikakkal, I. H. Aljundi, Mixed-Metal Cu-BTC Metal-Organic Frameworks as a Strong Adsorbent for Molecular Hydrogen at Low Temperatures, *ACS Omega* **5** (2020) 28493-28499. https://doi.org/10.1021/acsomega.0c02810
- [52] N. K. Gupta, J. Bae, K. -S. Kim, Role of Bimetallic Solutions in the Growth and Functionality of Cu-BTC Metal-Organic Framework, *Materials (Basel)* 15 (2022) 2804. https://doi.org/10.3390/ma15082804

- [53] J. Zhang, T. E, R. Zhou, N. Li, Y. Wang, Y. Li, S. Yang, Transition-state defect structure: A new strategy for TiO₂-based porous materials to enhance photodegradation of pollutants, *Journal of Environmental Management* **356** (2024) 120599. https://doi.org/10.1016/j.jenvman.2024.120599
- [54] S. Sanati, R. Abazari, A. M. Kirillov, Bimetallic NiCo Metal-Organic Frameworks with High Stability and Performance Toward Electrocatalytic Oxidation of Urea in Seawater, *Inorganic Chemistry* **63** (2024) 15813-15820. https://doi.org/10.1021/acs.inorgchem.4c01850
- [55] E. Özcan, Z. Mermer, Y. Zorlu, Metal-organic frameworks as photocatalysts in energetic and environmental applications, *Turkish Journal of Chemistry* 47 (2023) 1018-1052. https://doi.org/10.55730/1300-0527.3592
- [56] P. H. M. Andrade, H. Ahouri, C. Volkringer, T. Loiseau, H. Vezin, M. Hureau, A. Moissette, Electron-Donor Functional Groups, Band Gap Tailoring, and Efficient Charge Separation: Three Keys To Improve the Gaseous Iodine Uptake in MOF Materials, *ACS Applied Materials & Interfaces* **15** (2023) 31032-31048. https://doi.org/10.1021/acsami.3c04955
- [57] V. Poza-Nogueiras, E. Rosales, M. Pazos, M. Á. Sanromán, Current advances and trends in electro-Fenton process using heterogeneous catalysts A review, *Chemosphere* **201** (2018) 399-416. https://doi.org/10.1016/j.chemosphere.2018.03.002
- [58] L. H. Nguyen, H. T. Van, Q. N. Ngo, V. N. Thai, V. H. Hoang, N. T. T. Hai, Improving Fenton-like oxidation of Rhodamin B using a new catalyst based on magnetic/iron-containing waste slag composite, *Environmental Technology & Innovation* 23 (2021) 101582. https://doi.org/10.1016/j.eti.2021.101582
- [59] J. Fang, H. Yang, Q. Sun, T. Zhao, Evaluation of the remediation effect of solid waste synergistic materials on heavy metal-contaminated soil, *Journal of Environmental Chemical Engineering* **12** (2024) 114140. https://doi.org/10.1016/j.jece.2024.114140
- [60] J. Zhu, Efficient peroxydisulfate activation with γ-Al₂O₃-C-MIL-100(Fe) framework for sulfamethazine degradation: Enhanced oxidant utilization and reduced metal leaching, Applied Catalyst B: Environmental 359 (2025) 124520. https://doi.org/10.1016/j.apcatb.2024.124520
- [61] P. Kushwaha, M. Agarwal, A. Bhushan, Engineers Waste to waste treatment: Efficient upcycling of jarosite as a metal source and waste PET as a sustainable linker to synthesize iron-based MOF for wastewater treatment, *Journal of Taiwan Institute Chemical Engineers* **171** (2025) 106095. https://doi.org/10.1016/j.jtice.2025.106095
- [62] L. Q. Sun, X. F. Shen, H. M. Zhang, Y. H. Pang, Amino-functionalized iron-based MOFs for Rhodamine B degradation in heterogeneous photo-Fenton system, *Journal of Photochemistry and Photobiology A: Chemistry* 452 (2024) 115544. https://doi.org/10.1016/j.jphotochem.2024.115544
- [63] D. Terrón, A. Sanromán. Metal-Organic Frameworks: Next-Generation Materials for Environmental Remediation, *Catalysts* 15 (2025) 244. https://doi.org/10.3390/catal15030244
- [64] A. L. Pang, M. S. Iqbal, N. A. Rejab, U. Pal, M. A. S. M. Haniff, A. G. Ismail, A. A. Hamzah, Photocatalytic degradation of organic dye under UV light using CaCu₃Ti₄O₁₂ nanoparticles synthesized by sol gel route: Effect of calcination temperature, *Inorganic Chemistry Communications* **150** (2023) 110462. https://doi.org/10.1016/j.inoche.2023.110462
- [65] Y. S. Jara, T. T. Mekiso, A. P. Washe, Highly efficient catalytic degradation of organic dyes using iron nanoparticles synthesized with *Vernonia Amygdalina* leaf extract, *Scientific Reports* **14** (2024) 6997. https://doi.org/10.1038/s41598-024-57554-5
- [66] M. G. Kim, W. K. Song, J. S. Bae, Y. R. Cho, K. D. Song, Photocatalytic degradation of methylene blue under UV and visible light by brookite-rutile bi-crystalline phase of TiO₂, New Journal of Chemistry 45 (2021) 3485-3497. https://doi.org/10.1039/d0nj05162d



- [67] S. Y. Lee, H. S. Lim, N. E. Lee, S. O. Cho, Biocompatible UV-absorbing polymer nanoparticles prepared by electron irradiation for application in sunscreen, RSC Advances 10 (2019) 356-361. https://doi.org/10.1039/c9ra09752j
- [68] F. Zhang, J. Liu, H. Yue, G. Cheng, X. Xue, Enhanced photo-Fenton catalytic activity by spherical FeS₂ nanoparticles and photoelectric property of hybrid FeS₂/rGO, *Vacuum* **192** (2021) 110433. https://doi.org/10.1016/j.vacuum.2021.110433
- [69] Y. Mao, P. Wang, D. Zhang, Y. Xia, Y. Li, W. Zeng, S. Zhan, J. C. Crittenden, Accelerating Fe^{III}-Aqua Complex Reduction in an Efficient Solid-Liquid-Interfacial Fenton Reaction over the Mn-CNH Co-catalyst at Near-Neutral pH, *Environmental Science & Technology* **55** (2021) 13326-13334. https://doi.org/10.1021/acs.est.1c04534

©2025 by the authors; licensee IAPC, Zagreb, Croatia. This article is an open-access article distributed under the terms and conditions of the Creative Commons Attribution license (https://creativecommons.org/licenses/by/4.0/)